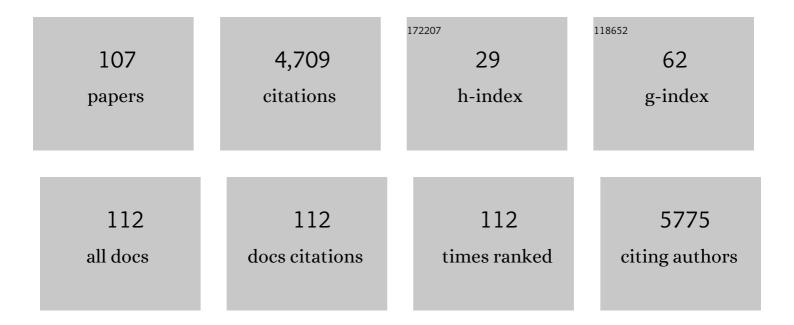
Marco Reisert

List of Publications by Year in descending order

Source: https://exaly.com/author-pdf/8493988/publications.pdf Version: 2024-02-01



#	Article	IF	CITATIONS
1	Gibbsâ€ringing artifact removal based on local subvoxelâ€shifts. Magnetic Resonance in Medicine, 2016, 76, 1574-1581.	1.9	918
2	Lead-DBS v2: Towards a comprehensive pipeline for deep brain stimulation imaging. NeuroImage, 2019, 184, 293-316.	2.1	527
3	Quantitative evaluation of 10 tractography algorithms on a realistic diffusion MR phantom. NeuroImage, 2011, 56, 220-234.	2.1	376
4	The structural–functional connectome and the default mode network of the human brain. NeuroImage, 2014, 102, 142-151.	2.1	283
5	Global fiber reconstruction becomes practical. NeuroImage, 2011, 54, 955-962.	2.1	277
6	Disentangling micro from mesostructure by diffusion MRI: A Bayesian approach. NeuroImage, 2017, 147, 964-975.	2.1	138
7	Global tractography of multi-shell diffusion-weighted imaging data using a multi-tissue model. Neurolmage, 2015, 123, 89-101.	2.1	128
8	Whole-Brain In-vivo Measurements of the Axonal G-Ratio in a Group of 37 Healthy Volunteers. Frontiers in Neuroscience, 2015, 9, 441.	1.4	97
9	The anatomy of the human medial forebrain bundle: Ventral tegmental area connections to reward-associated subcortical and frontal lobe regions. NeuroImage: Clinical, 2018, 18, 770-783.	1.4	93
10	Single shot whole brain imaging using spherical stack of spirals trajectories. NeuroImage, 2013, 73, 59-70.	2.1	90
11	The connectomics of brain demyelination: Functional and structural patterns in the cuprizone mouse model. NeuroImage, 2017, 146, 1-18.	2.1	83
12	Single shot concentric shells trajectories for ultra fast fMRI. Magnetic Resonance in Medicine, 2012, 68, 484-494.	1.9	81
13	The dentato-rubro-thalamic tract as the potential common deep brain stimulation target for tremor of various origin: an observational case series. Acta Neurochirurgica, 2020, 162, 1053-1066.	0.9	73
14	Intra-axonal diffusivity in brain white matter. NeuroImage, 2019, 189, 543-550.	2.1	71
15	Tractography-assisted deep brain stimulation of the superolateral branch of the medial forebrain bundle (sIMFB DBS) in major depression. NeuroImage: Clinical, 2018, 20, 580-593.	1.4	69
16	Deletion of the mu opioid receptor gene in mice reshapes the reward–aversion connectome. Proceedings of the National Academy of Sciences of the United States of America, 2016, 113, 11603-11608.	3.3	64
17	Three-dimensional MR-encephalography: Fast volumetric brain imaging using rosette trajectories. Magnetic Resonance in Medicine, 2011, 65, 1260-1268.	1.9	59
18	The absence of restricted water pool in brain white matter. NeuroImage, 2018, 182, 398-406.	2.1	59

#	Article	IF	CITATIONS
19	Tractographic description of major subcortical projection pathways passing the anterior limb of the internal capsule. Corticopetal organization of networks relevant for psychiatric disorders. NeuroImage: Clinical, 2020, 25, 102165.	1.4	52
20	Mapping remodeling of thalamocortical projections in the living <i>reeler</i> mouse brain by diffusion tractography. Proceedings of the National Academy of Sciences of the United States of America, 2013, 110, E1797-806.	3.3	51
21	Fiber Continuity: An Anisotropic Prior for ODF Estimation. IEEE Transactions on Medical Imaging, 2011, 30, 1274-1283.	5.4	50
22	Attentionâ€network specific alterations of structural connectivity in the undamaged white matter in acute neglect. Human Brain Mapping, 2014, 35, 4678-4692.	1.9	40
23	Distinct white matter alterations following severe stroke. Neurology, 2017, 88, 1546-1555.	1.5	40
24	Joint Imaging Platform for Federated Clinical Data Analytics. JCO Clinical Cancer Informatics, 2020, 4, 1027-1038.	1.0	39
25	Quantification and correction of respiration induced dynamic field map changes in fMRI using 3D single shot techniques. Magnetic Resonance in Medicine, 2014, 71, 1093-1102.	1.9	38
26	Probing the reproducibility of quantitative estimates of structural connectivity derived from global tractography. NeuroImage, 2018, 175, 215-229.	2.1	35
27	A unique analytical solution of the white matter standard model using linear and planar encodings. Magnetic Resonance in Medicine, 2019, 81, 3819-3825.	1.9	35
28	Fast Rotation Invariant 3D Feature Computation Utilizing Efficient Local Neighborhood Operators. IEEE Transactions on Pattern Analysis and Machine Intelligence, 2012, 34, 1563-1575.	9.7	32
29	Frontal white matter architecture predicts efficacy of deep brain stimulation in major depression. Translational Psychiatry, 2019, 9, 197.	2.4	32
30	The ventral pathway of the human brain: A continuous association tract system. NeuroImage, 2021, 234, 117977.	2.1	32
31	About the Geometry of Asymmetric Fiber Orientation Distributions. IEEE Transactions on Medical Imaging, 2012, 31, 1240-1249.	5.4	30
32	MesoFT: Unifying Diffusion Modelling and Fiber Tracking. Lecture Notes in Computer Science, 2014, 17, 201-208.	1.0	30
33	Widespread white matter oedema in subacute COVID-19 patients with neurological symptoms. Brain, 2022, 145, 3203-3213.	3.7	25
34	Effects of mesoscopic susceptibility and transverse relaxation on diffusion NMR. Journal of Magnetic Resonance, 2018, 293, 134-144.	1.2	24
35	Machine learning—aided personalized DTI tractographic planning for deep brain stimulation of the superolateral medial forebrain bundle using HAMLET. Acta Neurochirurgica, 2019, 161, 1559-1569.	0.9	24
36	Second order 3D shape features: An exhaustive study. Computers and Graphics, 2006, 30, 197-206.	1.4	21

#	Article	IF	CITATIONS
37	Arterial input function measurements for bolus tracking perfusion imaging in the brain. Magnetic Resonance in Medicine, 2013, 69, 771-780.	1.9	21
38	MITK global tractography. Proceedings of SPIE, 2012, , .	0.8	20
39	Predicting Planning Performance from Structural Connectivity Between Left and Right Mid-Dorsolateral Prefrontal Cortex: Moderating Effects of Age During Postadolescence and Midadulthood. Cerebral Cortex, 2015, 25, 869-883.	1.6	20
40	Complex Derivative Filters. IEEE Transactions on Image Processing, 2008, 17, 2265-2274.	6.0	18
41	Molecular Imaging of Activated Platelets Allows the Detection of Pulmonary Embolism with Magnetic Resonance Imaging. Scientific Reports, 2016, 6, 25044.	1.6	18
42	Voxel-wise deviations from healthy aging for the detection of region-specific atrophy. NeuroImage: Clinical, 2018, 20, 851-860.	1.4	18
43	Equivariant Holomorphic Filters for Contour Denoising and Rapid Object Detection. IEEE Transactions on Image Processing, 2008, 17, 190-203.	6.0	17
44	3D CMRO2 mapping in human brain with direct 17O MRI: Comparison of conventional and proton-constrained reconstructions. NeuroImage, 2017, 155, 612-624.	2.1	17
45	Connectivity of the Superficial Muscles of the Human Perineum: A Diffusion Tensor Imaging-Based Global Tractography Study. Scientific Reports, 2018, 8, 17867.	1.6	16
46	PAT—Probabilistic Axon Tracking for Densely Labeled Neurons in Large 3-D Micrographs. IEEE Transactions on Medical Imaging, 2019, 38, 69-78.	5.4	16
47	Diverging prefrontal cortex fiber connection routes to the subthalamic nucleus and the mesencephalic ventral tegmentum investigated with long range (normative) and short range (ex-vivo) Tj ETQq1	1 01728431	4 ngßT /Overl
48	Harmonic Filters for 3D Multichannel Data: Rotation Invariant Detection of Mitoses in Colorectal Cancer. IEEE Transactions on Medical Imaging, 2010, 29, 1485-1495.	5.4	15
49	Fiber density estimation from single q-shell diffusion imaging by tensor divergence. NeuroImage, 2013, 77, 166-176.	2.1	15
50	Optimization and validation of diffusion MRI-based fiber tracking with neural tracer data as a reference. Scientific Reports, 2020, 10, 21285.	1.6	15
51	Brain network remodelling reflects tau-related pathology prior to memory deficits in Thy-Tau22 mice. Brain, 2020, 143, 3748-3762.	3.7	15
52	MR image reconstruction from generalized projections. Magnetic Resonance in Medicine, 2014, 72, 546-557.	1.9	14
53	SVM-Based Normal Pressure Hydrocephalus Detection. Clinical Neuroradiology, 2021, 31, 1029-1035.	1.0	14
54	Diffusion Tensor Imaging Reveals Whole-Brain Microstructural Changes in the P301L Mouse Model of Tauopathy. Neurodegenerative Diseases, 2020, 20, 173-184.	0.8	14

#	Article	IF	CITATIONS
55	SHOG - Spherical HOG Descriptors for Rotation Invariant 3D Object Detection. Lecture Notes in Computer Science, 2011, , 142-151.	1.0	12
56	Assessment of spinal cord motion as a new diagnostic MRI-parameter in cervical spinal canal stenosis: study protocol on a prospective longitudinal trial. Journal of Orthopaedic Surgery and Research, 2019, 14, 321.	0.9	12
57	Spinal Cord Motion in Degenerative Cervical Myelopathy: The Level of the Stenotic Segment and Gender Cause Altered Pathodynamics. Journal of Clinical Medicine, 2021, 10, 3788.	1.0	12
58	Increased interstitial fluid in periventricular and deep white matter hyperintensities in patients with suspected idiopathic normal pressure hydrocephalus. Scientific Reports, 2021, 11, 19552.	1.6	12
59	Revealing signal from noisy ¹⁹ F MR images by chemical shift artifact correction. Magnetic Resonance in Medicine, 2015, 73, 2225-2233.	1.9	11
60	Automated Infarct Core Volumetry Within the Hypoperfused Tissue. Journal of Computer Assisted Tomography, 2017, 41, 515-520.	0.5	11
61	Hippocampus-Avoidance Whole-Brain Radiation Therapy Is Efficient in the Long-Term Preservation of Hippocampal Volume. Frontiers in Oncology, 2021, 11, 714709.	1.3	11
62	Harmonic Filters for Generic Feature Detection in 3D. Lecture Notes in Computer Science, 2009, , 131-140.	1.0	11
63	Autoimmune Obsessive-Compulsive Disorder with Novel Anti-Basal Ganglia Antibodies. Psychotherapy and Psychosomatics, 2022, 91, 214-216.	4.0	10
64	Efficient Monte Carlo Image Analysis for the Location of Vascular Entity. IEEE Transactions on Medical Imaging, 2015, 34, 628-643.	5.4	9
65	Spherical Tensor Algebra: A Toolkit for 3D Image Processing. Journal of Mathematical Imaging and Vision, 2017, 58, 349-381.	0.8	9
66	Spherical Tensor Calculus for Local Adaptive Filtering. Advances in Pattern Recognition, 2009, , 153-178.	0.8	9
67	Invariant features for searching in protein fold databases. International Journal of Computer Mathematics, 2007, 84, 635-651.	1.0	8
68	Focal cervical spinal stenosis causes mechanical strain on the entire cervical spinal cord tissue – A prospective controlled, matched-pair analysis based on phase-contrast MRI. NeuroImage: Clinical, 2021, 30, 102580.	1.4	8
69	Blood Tracer Kinetics in the Arterial Tree. PLoS ONE, 2014, 9, e109230.	1.1	7
70	Initial investigation of glucose metabolism in mouse brain using enriched ¹⁷ O-glucose and dynamic ¹⁷ O-MRS. NMR in Biomedicine, 2017, 30, e3724.	1.6	7
71	Modelfree global tractography. NeuroImage, 2018, 174, 576-586.	2.1	7
72	Direct estimation of ¹⁷ O MR images (DIESIS) for quantification of oxygen metabolism in the human brain with partial volume correction. Magnetic Resonance in Medicine, 2018, 80, 2717-2725.	1.9	7

#	Article	IF	CITATIONS
73	Fully automated detection of focal cortical dysplasia: Comparison of MPRAGE and MP2RAGE sequences. Epilepsia, 2022, 63, 75-85.	2.6	7
74	Diffusion Microstructure Imaging to Analyze Perilesional T2 Signal Changes in Brain Metastases and Glioblastomas. Cancers, 2022, 14, 1155.	1.7	7
75	DTI for brain targeting: Diffusion weighted imaging fiber tractography—Assisted deep brain stimulation. International Review of Neurobiology, 2021, 159, 47-67.	0.9	6
76	"Within a minute―detection of focal cortical dysplasia. Neuroradiology, 2022, 64, 715-726.	1.1	6
77	Atri-U: assisted image analysis in routine cardiovascular magnetic resonance volumetry of the left atrium. Journal of Cardiovascular Magnetic Resonance, 2021, 23, 133.	1.6	6
78	Diffusion microstructure imaging in progressive supranuclear palsy: reduced axonal volumes in the superior cerebellar peduncles, dentato-rubro-thalamic tracts, ventromedial thalami, and frontomesial white matter. Cerebral Cortex, 2022, 32, 5628-5636.	1.6	6
79	Automated segmentation of head CT scans for computer-assisted craniomaxillofacial surgery applying a hierarchical patch-based stack of convolutional neural networks. International Journal of Computer Assisted Radiology and Surgery, 2022, 17, 2093-2101.	1.7	6
80	Quantitative cerebral blood flow with bolus tracking perfusion MRI: Measurements in porcine model and comparison with PET. Magnetic Resonance in Medicine, 2014, 72, 1723-1734.	1.9	5
81	Approximation to painâ€signaling network in humans by means of migraine. Human Brain Mapping, 2021, 42, 766-779.	1.9	5
82	Mapping the living mouse brain neural architecture: strain-specific patterns of brain structural and functional connectivity. Brain Structure and Function, 2021, 226, 647-669.	1.2	5
83	3D X-ray based visualization of directional deep brain stimulation lead orientation. Journal of Neuroradiology, 2021, , .	0.6	5
84	Fiber Continuity Based Spherical Deconvolution in Spherical Harmonic Domain. Lecture Notes in Computer Science, 2013, 16, 493-500.	1.0	5
85	Arterial input function in a dedicated slice for cerebral perfusion measurements in humans. Magnetic Resonance Materials in Physics, Biology, and Medicine, 2018, 31, 439-448.	1.1	4
86	Support Vector Machine-based Spontaneous Intracranial Hypotension Detection on Brain MRI. Clinical Neuroradiology, 2022, 32, 225-230.	1.0	4
87	Diffusion tensor imaging in unclear intramedullary tumor-suspected lesions allows separating tumors from inflammation. Spinal Cord, 2022, 60, 655-663.	0.9	4
88	Spherical Bessel Filter for 3D object detection. , 2011, , .		3
89	Data on the test-retest reproducibility of streamline counts as a measure of structural connectivity. Data in Brief, 2018, 19, 1361-1381.	0.5	3
90	Discrimination of epileptogenic lesions and perilesional white matter using diffusion tensor magnetic resonance imaging. Neuroradiology Journal, 2019, 32, 10-16.	0.6	3

#	Article	IF	CITATIONS
91	SPECTRE —A novel dMRI visualization technique for the display of cerebral connectivity. Human Brain Mapping, 2021, 42, 2309-2321.	1.9	3
92	Atlas-Guided Global Tractography: Imposing a Prior on the Local Track Orientation. Mathematics and Visualization, 2014, , 115-123.	0.4	3
93	Novel anti-cytoplasmic antibodies in cerebrospinal fluid and serum of patients with chronic severe mental disorders. World Journal of Biological Psychiatry, 2022, 23, 794-801.	1.3	3
94	Is microdiffusion imaging able to improve the detection of cervical myelopathy? Study protocol of a prospective observational trial (MIDICAM-Trial). BMJ Open, 2019, 9, e029153.	0.8	2
95	Contrast Bolus Interference in a Multimodal CT Stroke Protocol. American Journal of Neuroradiology, 2021, 42, 1807-1814.	1.2	2
96	Reduced structural connectivity in the corpus callosum in patients with anorexia nervosa. European Eating Disorders Review, 2022, , .	2.3	2
97	A Neuroanatomy of Positive Affect Display – Subcortical Fiber Pathways Relevant for Initiation and Modulation of Smiling and Laughing. Frontiers in Behavioral Neuroscience, 2022, 16, 817554.	1.0	2
98	Altered transcallosal fiber count and volume in high-functioning adults with autism spectrum disorder. Psychiatry Research - Neuroimaging, 2022, 322, 111464.	0.9	2
99	Biomechanical Effects of Chronic Ankle Instability on the Talar Cartilage Matrix: The Value of T1Ï• Relaxation Mapping Without and With Mechanical Loading. Journal of Magnetic Resonance Imaging, 2023, 57, 611-619.	1.9	2
100	Rotation Covariant Image Processing for Biomedical Applications. Computational and Mathematical Methods in Medicine, 2013, 2013, 1-19.	0.7	1
101	Robust intra-individual estimation of structural connectivity by Principal Component Analysis. NeuroImage, 2021, 226, 117483.	2.1	1
102	Cross-Correlation and Rotation Estimation of Local 3D Vector Field Patches. Lecture Notes in Computer Science, 2009, , 287-296.	1.0	1
103	Steerable Deconvolution Feature Detection as an Inverse Problem. Lecture Notes in Computer Science, 2011, , 326-335.	1.0	1
104	Alpha helix prediction based on Metropolis-Hastings sampling. , 2011, , .		0
105	There's more to the picture than meets the eye. Acta Neurochirurgica, 2020, 162, 1869-1870.	0.9	0
106	Fiber Density Estimation by Tensor Divergence. Lecture Notes in Computer Science, 2012, 15, 297-304.	1.0	0
107	Efficient Metropolis-Hasting Image Analysis for the Location of Vascular Entity. Lecture Notes in Computer Science, 2014, , 421-431.	1.0	0